Understanding the injection process of hydrogen on Pt$_1$-TiO$_2$ surface for photocatalytic hydrogen evolution

Zhenggang Xue [a], Muyu Yan [b], Yida Zhang [c], Jiaqiang Xu [a], Xiaoping Gao [b,*], Yuen Wu [b,*]

[a] *NEST Lab., Department of Physics, College of Science, Shanghai University, 99 Shangda Road, Shanghai 200444, China*
[b] *Hefei National Laboratory for Physical Sciences at the Microscale, Collaborative Innovation Center of Chemistry for Energy Materials (iChEM), School of Chemistry and Materials Science, and National Synchrotron Radiation Laboratory, University of Science and Technology of China, Hefei 230026, China*
[c] *National Synchrotron Radiation Laboratory, University of Science and Technology of China , Hefei 230026, China*

A B S T R A C T

Observing and understanding the surface changes of catalysts during reactive process can provide imperative insights into the mechanism study. Here, we investigated several different surface behaviors based on Pt/TiO$_2$ catalysts during photocatalytic hydrogen evolution process. We found the single Pt atoms on TiO$_2$ surface (Pt$_1$-TiO$_2$) could induce the hydrogen injection into the TiO$_2$ subsurface to generate self-hydrogenated shell. This hydrogenated configurations in subsurface can serve as dominated locations for hydrogen formation and desorption process, which greatly boost the catalytic rate. Electron energy loss spectroscopy and in-situ experiments further confirm the as-formed amorphous shell contains reduced Ti ions and oxygen defects. Density functional theory calculations verify that high-concentrated hydrogenated shell on Pt$_1$-TiO$_2$ surface can significantly reduce the desorption energies of H$_2$ formation. Our discovery thus provides important insight for the fundamental understanding of hydrogen evolution reactions and is also expected to open up a new way to design highly effective photocatalysts.

1. Introduction

Photocatalytic conversion of solar energy to renewable clean energy (e.g., H$_2$) is a promising approach to address both energy crisis and environmental challenges [1–5]. One of bottlenecks for developing highly efficient photocatalysts is to deeply understand the reaction pathways happened at the material surface during photocatalytic process. Since the photocatalytic water splitting was discovered in 1972, TiO$_2$-based photocatalysts have attracted extensive interests [6,7]. For example, recent study has shown the hydroxylated amorphous layer with several layer thicknesses will form and cover on the anatase TiO$_2$ surface under UV light irradiation in water vapor [8]. This behavior of flowing hydrogen atoms into the subsurface of TiO$_2$ thus focused extensive concerns [9–11]. And the surface-related transformation typically leads to the changes of adsorption and desorption energies for hydrogen evolution. Besides, the amorphous surfaces also have been widely proved that the disordered atomic arrangements will expose more unsaturated sites to adsorb and dissociate H$_2$O molecules and enhance the hydrogen evolution performances [12–14]. When the noble metal nanoparticles (such as, Pt or Pd) are further loaded as co-catalysts

on the TiO$_2$ surface, the photoexcited electrons can be transferred from TiO$_2$ conduction band to the co-catalyst surface, which profoundly enhance the separation efficiency of charge carriers and electron transport rate [15–20]. Meanwhile, the process will lead the adsorption and activation of hydrogen predominantly focus on metal sites [21]. To further improve the photocatalytic properties, downsizing metal co-catalysts sizes into single atoms can fully expose active surface of photocatalysts. Also, the unique electronic configuration and spatial isolation may confer the single-atom sites catalysts (SACs) with special reaction pathways and unexpected photocatalytic performances [22–25]. However, the atomic level investigation of surface changes for SACs occurring in photocatalytic environment have rarely been studied, resulting into the reaction pathways and mechanisms are still elusive. The lack of fundamental understanding for surface structure-reactivity relations is thus considered as a major challenge for increasing the photocatalytic performances.

Herein, we investigated several evolution processes of metal Pt on TiO$_2$ surface during photocatalytic hydrogen evolution. We found, for Pt single-atom loading TiO$_2$ nanosheets (Pt$_1$-TiO$_2$ NSs) catalysts, surface single Pt atoms trend to induce the hydrogen injection into the TiO$_2$

subsurface to generate self-hydrogenated shell during photocatalytic process. The resultant amorphous layer gradually propagated towards the center of TiO₂ NSs and finally stabilized with a thickness of about 2 nm. Electron energy loss spectroscopy (EELS) and the in-situ electron paramagnetic resonance (EPR) measurements confirm the shell structure contains reduced Ti ions and coexisting oxygen defects. In contrast, no obvious self-hydrogenated shell is observed in both bare TiO₂ NSs and Pt nanoparticles loading TiO₂ NSs (Pt-NP-TiO₂ NSs) catalysts after photocatalytic reactions. Experimental photoelectrochemical characterizations and density functional theory (DFT) calculations further verify that single atom Pt on TiO₂ surface can effectively facilitate the permeation of hydrogen to the subsurface and ultimately induce the formation of hydrogenated shell, which reduces the desorption energies of H_2 evolution. The final Pt_1-TiO₂ catalysts show excellent photocatalytic activity of 42.9 mmol g^{-1} h^{-1}, exceeding the Pt-NP-TiO₂ NSs catalysts (8.8 mmol g^{-1} h^{-1}), pure TiO₂ (0.5 mmol g^{-1} h^{-1}) and most reported photocatalysts.

2. Experimental section

2.1. Preparation of samples

2.1.1. Preparation of TiO₂ NSs

TiO₂ NSs were prepared by the hydrothermal method. Typically, 0.8 mL of hydrofluoric acid solution (40 wt%) was mixed with the 5 mL of Ti (OBu)₄●(TBOT) under stirring. After stirring for 2 h, the mixture gel was collected and transferred into a sealed Teflon autoclave and then kept at 200 °C for 24 h. After cooling down, the product was separated by washed with ethanol and distilled water several times. At last, the resulting TiO₂ powder was dried at 60 °C over a night for further characterization.

2.1.2. Preparation of Pt-TiO₂ NSs with various concentrations

In a typical procedure, 100 mg TiO₂ NSs powders were dispersed and ultrasound in 20 mL water for 20 min. After stirring for 2 h, a certain amount of H_2PtCl_6 aqueous solution (Pt: 4 mg/mL) was then added into the stock solution. After stirring for 4 h, the as-formed precipitates were washed with water for several times and dried at 80 °C under vacuum.

2.1.3. Preparation of Pt-NP-TiO₂ NSs

In a typical procedure, 100 mg TiO₂ NSs powders were dispersed and ultrasound in 20 mL water for 20 min. After stirring for 2 h, 0.125 mL H_2PtCl_6 aqueous solution (Pt: 4 mg/mL) and sodium borohydride were then added into the stock solution. After stirring for 2 h, the as-formed precipitates were washed with water for several times and dried at 60 °C under vacuum.

2.2. Characterization

2.2.1. Materials characterization

Powder X-ray diffraction (XRD) measurements were recorded on a Rigaku Miniflex-600 operated at 40 kV voltage and 15 mA current using a Cu Kα radiation (λ = 0.15406 nm) at a step width of 8°/min. The SEM was performed on JSM-6700 F. TEM images were recorded on a Hitachi-7700 worked at 100 kV. The high-resolution TEM, HAADF-STEM images were recorded on a FEI Tecnai G2 F20 S-Twin high-resolution transmission electron microscope worked at 200 kV and a JEOL JEM-ARM200F TEM/STEM with a spherical aberration corrector worked at 300 kV. Through-focal HAADF series were acquired at nanometer intervals, with the first image under-focused (beyond the beam exit surface) and the final image over-focused (before the beam entrance surface). The images were then manually aligned to remove the sample drift effects. XPS experiments were performed at the Catalysis and Surface Science End station at the BL11U beamline of National Synchrotron Radiation Laboratory (NSRL) in Hefei, China. Near ambient pressure X-ray photoelectron spectroscopy (NAP-XPS) was conducted on

equipment manufactured by SPECS Surface Nano Analysis GmbH, Germany. The analysis chamber included a microfocus monochromatized Al Kα X-ray source, a PHOIBOS NAP hemispherical electron energy analyser, a SPECS IQE-11A ion gun, and an infrared laser heater. The powdered samples dissolved in the mixed liquor of water and triethanolamine were dropped onto a copper foil and dried at room temperature. The measurements were performed under 1 mbar air under a 300 W Xe lamp irradiation. Photoluminescent (PL) spectra were acquired on a Horiba YJ Fluorolog-3-tau Steady-state spectrofluorometer. UV−vis absorption spectra were collected by an Agilent Cary 60 spectrophotometer. Room-temperature EPR spectra were obtained using a JEOL JES-FA200 spectrometer (300 K, 9.062 GHz). Raman scattering spectra were recorded with a Renishaw System 2000 spectrometer using the 514.5 nm line of Ar^+ for excitation.

2.2.2. XAFS characterization

XAFS measurement and data analysis: The X-ray absorption find structure data were collected at 1W1B station in Beijing Synchrotron Radiation Facility (BSRF). The storage rings of BSRF was operated at 2.5 GeV with a maximum current of 250 mA. The XANES data were recorded in a fluorescence mode. All samples were pelletized as disks of 13 mm diameter using poly(1,1-difluoroethylene) powder as a binder. The acquired EXAFS data were processed according to the standard procedures using the ATHENA module implemented in the IFEFFIT software packages. The EXAFS spectra were obtained by subtracting the post-edge background from the overall absorption and then normalizing with respect to the edge-jump step. Subsequently, χ(k) data in the k-space were Fourier transformed to real (R) space using a hanning windows (dk=1.0 Å^{-1}) to separate the EXAFS contributions from different coordination shells.

2.3. Photocatalytic H_2 production test

The photocatalytic hydrogen experiments were performed in a 50 mL quartz reactor at 25 °C and atmospheric pressure. A 300 W Xe lamp was used as the UV–visible light source. For the typical experiment, 5 mg of photocatalysts were suspended in 10 mL of mixture solvent (H_2O/triethanolamine) with a volume ratio of 9:1. The quartz reactor was then thoroughly degassed and backfilled with pure Ar_2 three times before the irradiation. The gaseous products were analyzed by an on-line gas chromatograph (PANNA A91).

3. Results and discussion

3.1. Synthesis and characterization of Pt-TiO₂ NSs

The TiO₂ NSs were firstly prepared via a simple solvothermal process. The transmission electron microscopy (TEM) image in Fig. S1a reveals the TiO₂ NSs structure with a width of 40–75 nm. The high-resolution transmission electron microscopy (HRTEM) images in Fig. S1b display well-defined lattice fringes of TiO₂ NSs. Moreover, the bulk and edge regions are clearly-resolved and well-crystallized without notable distortion and defects. Subsequently, the platinum species were further decorated on TiO₂ NSs through a post-modification strategy by precisely controlling the adding rates of precursors (see Experimental Procedures). As shown in Fig. S2, no obvious Pt nanoparticles are observed when the Pt loadings are not higher than 0.5 wt%. While the Pt nanoparticles quantitatively increase as the metal loadings continually enhance. This can be further corroborated by the mapping images in Fig. S3 and S4. The High-angle-annular-dark-field scanning transmission electron microscopy (HAADF-STEM) image shown in Fig. 1a exhibits amounts of clearly visible dots (circled in Fig. 1a) in 0.5 wt% Pt-TiO₂ catalysts (named as Pt_1-TiO₂), which can be assigned to isolated single Pt atoms. Based on the experimental STEM image (Fig. 1b, extracted from green rectangle in Fig. 1a), the simulating configuration (Fig. 1c) sufficiently confirms the presence of single Pt atoms. Meanwhile, no obvious
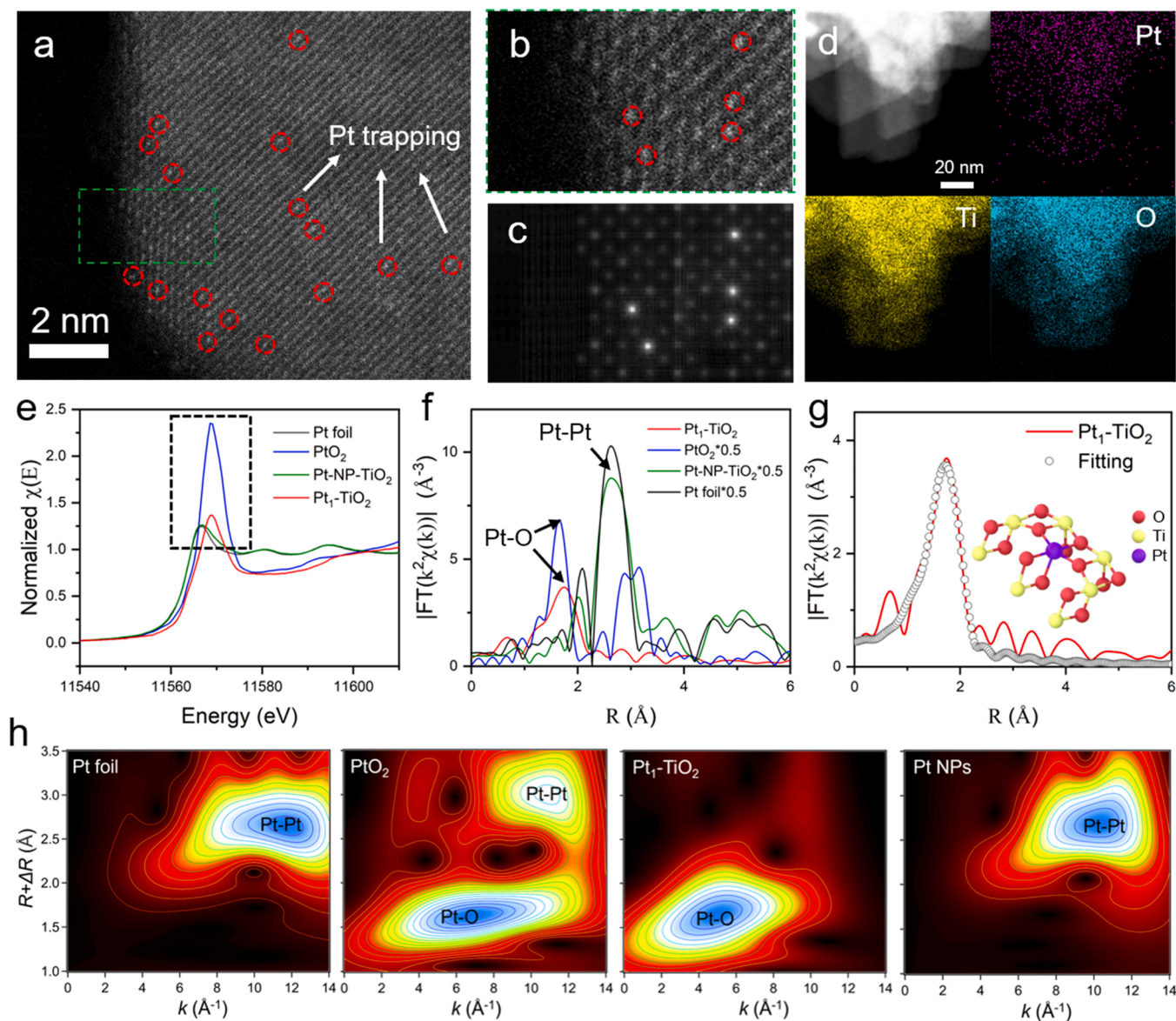
Fig. 1. (a) HAADF-STEM image of Pt$_1$-TiO$_2$. Amplifying image (b) and simulated image (c) of green frame in (a). The Pt atoms are marked by red circles. (d) EDS elemental mapping of Pt$_1$-TiO$_2$. (e) The Pt L-edge XANES spectra. (f) The EXAFS spectra and (g) corresponding fitting curve of Pt L$_3$ edge. (h) Wavelet transform patterns of Pt foil, PtO$_2$, Pt$_1$-TiO$_2$, Pt NPs.

signals of Pt particles are detected in X-ray diffraction (XRD) patterns (Fig. S5). Furthermore, the energy-dispersive X-ray spectroscopy (EDS) mapping in Fig. 1d reveals the homogeneous distribution of Pt species without obvious agglomeration over the whole Pt$_1$-TiO$_2$ NSs.

In order to further verify the local environment and structure around the Pt sites in Pt$_1$-TiO$_2$, the X-ray absorption near-edge structure (XANES) measurements were implemented. As seen in Fig. 1e, the intensity of white line peak for Pt$_1$-TiO$_2$ is higher than the Pt foil but lower than PtO$_2$, suggesting the slightly positive charges nature of Pt atoms. The same results can be further validated by the X-ray photoelectron spectroscopy (XPS) analysis in Fig. S6, in which the Pt binding energy is between Pt nanoparticles (Pt^0, at ~71.2 eV) and PtO$_2$ (Pt^{4+}, at ~74.0 eV). The extended X-ray absorption fine structure (EXAFS) spectrum in Fig. 1f shows the short-range local structure of Pt in Pt$_1$-TiO$_2$ samples. Only one prominent Pt-O shell peak at about 1.8 Å can be discovered and the Pt-Pt shell at 2.7 Å is absent, demonstrating the single atomic Pt site configuration. Meanwhile, the wavelet transform (WT) contour plots of Pt L-edge EXAFS oscillations in Fig. 1h depict two main peak at 6 and 11 Å^{-1}, which are respectively ascribed to the Pt-O

and Pt-Pt contribution. Impressively, the Pt$_1$-TiO$_2$ shows only one Pt-O peak at 5 Å^{-1}, indicating the Pt species are atomically dispersed over Pt$_1$-TiO$_2$ supports. Furthermore, the according EXAFS fitting curve (Fig. 1g) and fitting parameters (Table S1) indicate that the coordination numbers of Pt in Pt$_1$-TiO$_2$ is about 4.7 and the average bond length is 1.97 Å.

3.2. Photocatalytic H$_2$ evolution reaction

The photocatalytic H$_2$ evolution reaction was investigated under a 300 W Xe lamp irradiation with triethanolamine as a hole scavenger. After the decoration of Pt species, all the synthesized samples show remarkably enhanced photocatalytic performances compared to pure TiO$_2$ (Fig. 2a). Especially, the highest photocatalytic activity of 42.9 mmol g^{-1} h^{-1} is reached when the Pt metal loading arrives to 0.5 wt%, which is 86 times higher activity than pure TiO$_2$ (0.5 mmol g^{-1} h^{-1}). To our best knowledge, the photocatalytic H$_2$ production activity of Pt$_1$-TiO$_2$ catalyst surpasses that of most reported photocatalysts (Fig. 2e and Table S2). Moreover, the rate of H$_2$ evolution of Pt$_1$-TiO$_2$
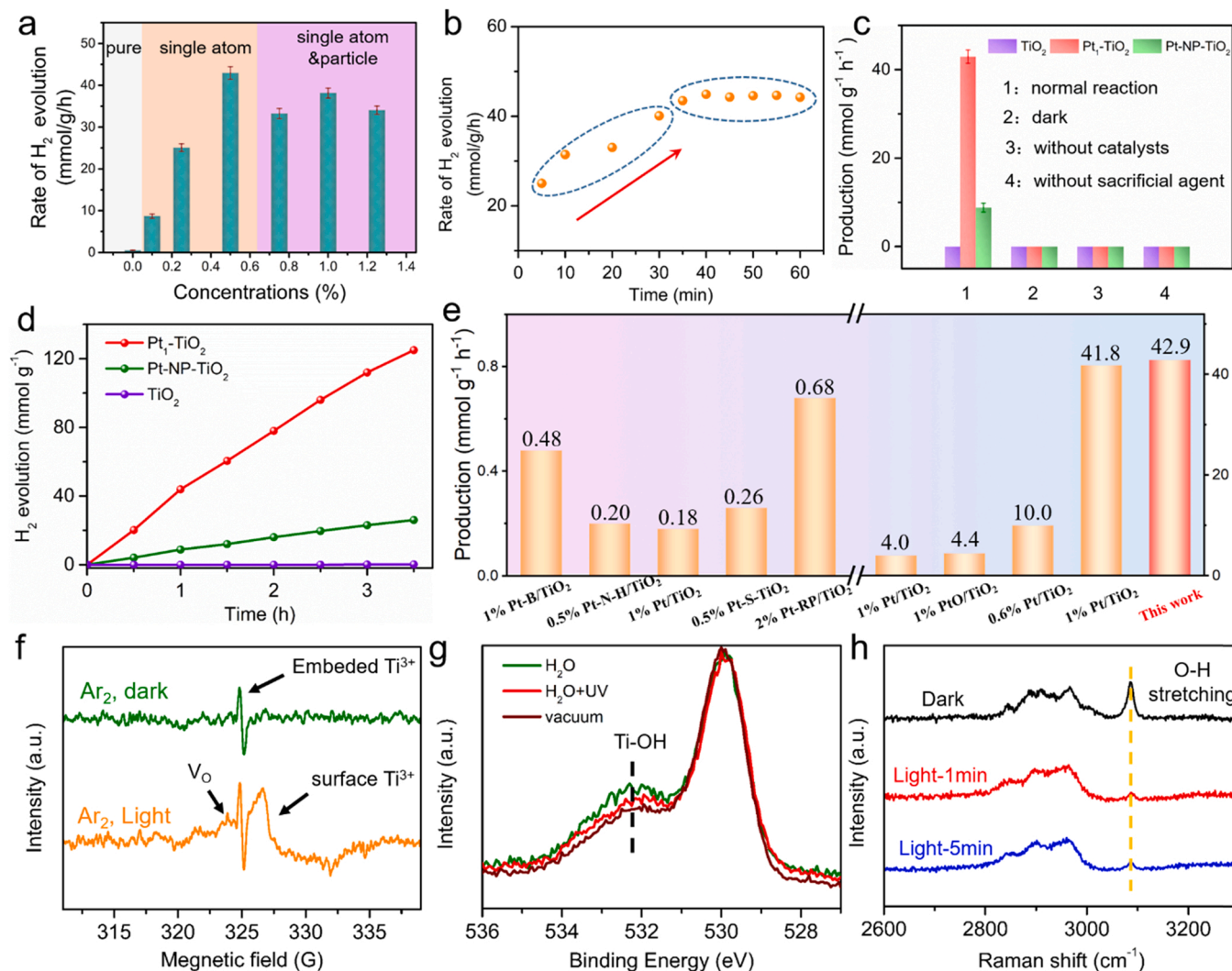
Fig. 2. (a) Photocatalytic H_2 generation rates for various concentrations Pt loading TiO_2 NSs. (b) Comparison of H_2 evolution rates for Pt_1-TiO_2 at different time. (c) The control experiments of photocatalytic H_2 rate for TiO_2, Pt_1-TiO_2 and Pt-NP-TiO_2 catalysts under altered conditions. (d) Time-dependent photocatalytic H_2 production within 3.5 h using TiO_2, Pt_1-TiO_2 and Pt-NP-TiO_2 catalysts. (e) Comparison of photocatalytic H_2 production performance over Pt_1-TiO_2 and other photocatalysts reported in the literatures (Table S2). (f) In-situ EPR spectra of Pt_1-TiO_2 under various conditions. (g) In-situ O 1 s XPS spectra and (h) Ex-situ Raman spectra of Pt_1-TiO_2 under various simulative photocatalytic conditions.

readily enhanced within 30 min once the light irradiation, and then the value of rate will remain nearly constant (Fig. 2b). Therefore, the adsorption of water molecules, reaction and desorption of hydrogen process could be rapidly implemented and reach a dynamic equilibrium within 30 min. Control experiments in Fig. 2c exhibit that no hydrogen products in the absence of light, catalysts and sacrificial agent, suggesting a real photocatalytic process involving the H_2O as the proton source and Pt_1-TiO_2 materials as the photosensitizer. For comparison, the 0.5 wt% Pt nanoparticles loading TiO_2 NSs (named as Pt-NP-TiO_2, Fig. S7), prepared by a direct reduction process using sodium borohydride, displays a hydrogen evolution rate of 8.8 mmol g^{-1} h^{-1}, which is pronouncedly lower than Pt_1-TiO_2 catalysts under same condition. In addition, the photocatalytic hydrogen production linearly increases with the irradiation time and no noticeable decrease during 3.5 h test (Fig. 2d). Meanwhile, the time-circle hydrogen evolution experiments of three samples were implemented in Fig. S8. No obvious sign degradations are observed after three cycles and the H_2 evolution performances still remain stable after two weeks, indicating the excellent stability. Photo-electrochemical measurements were further conducted to exposit the excellent hydrogen photo-reduction performances of Pt_1-TiO_2. As shown in Fig. S9a, the introduction of Pt single atoms significantly

suppresses electron-hole recombination, leading into a lower emission steady-state photoluminescence (PL) intensity. Meanwhile, the photocurrent densities of Pt_1-TiO_2 NSs are significantly increased compared to pure TiO_2 and Pt-NP-TiO_2 samples (Fig. S9b), demonstrating the superb transport features of photogenerated charges. In addition, UV–vis diffuse reflectance spectra and band gap results in Fig. S10 show stronger absorption and narrower band gap of Pt_1-TiO_2 NSs relative to TiO_2 and Pt-NP-TiO_2.

3.3. Photocatalytic mechanisms

The in-situ electron paramagnetic resonance (EPR) measurements were further conducted to explore the hydrogen evolution process over the Pt_1-TiO_2 surface. As seen in Fig. 2f, only one EPR peak at g= 1.98 of Pt_1-TiO_2 sample is found in the darkness condition, which is associated to the typical lattice-embedded Ti^{3+} centers [26]. On light irradiation, the surface exposed Ti^{3+} and oxygen defects signals appear with dominant resonance g values of 1.94 and 2.003 respectively. This strongly suggests that hydrogen evolution process could induce more surface exposed Ti^{3+} and oxygen defects on the Pt_1-TiO_2 surface. For TiO_2 catalysts during photocatalytic process, the surface Ti^{3+} species enhance

under the light condition, while the change in valences of TiO$_2$ will not lead obvious structure changes on TiO$_2$ surface (Fig. S11a). However, no obvious peak changes are founded for Pt-NP-TiO$_2$ samples before and after light irradiation (Fig. S11b). Furthermore, the changes of oxygen element in Pt$_1$-TiO$_2$ samples were recorded by in-situ near ambient pressure XPS spectra performed under simulative hydrogen evolution conditions. As shown in Fig. 2g, two obvious O 1 s peaks located at 529.97 eV and 532.02 eV can be discovered in vacuum condition, which are assigned to Ti-O-Ti lattice oxygen and Ti-OH surface hydroxyl [27], respectively. After H$_2$O treatment under near ambient pressure, the peak intensity of surface hydroxyl significantly increases, which is attributed to H$_2$O molecules adsorbed on the Pt$_1$-TiO$_2$ surface. When further light irradiation, the signal of surface hydroxyl decreases due to the hydrogen evolution process. Interestingly, the intensity of hydroxyl peak is still higher than that in vacuum condition, which may be caused by the oxygen defects on the surface to contribute hydroxyl surface groups [24]. The ex-situ Raman spectrum was further implemented to investigate the interfacial properties of Pt$_1$-TiO$_2$ catalysts. The prominent band at ca. 3100 cm^{-1} in Fig. 2h is ascribed to the O-H stretching mode of water molecules [28]. After light treatment, the intensity shows an evident decrease, indicating the rapid photocatalytic H$_2$O splitting process on the Pt$_1$-TiO$_2$ surface.

To further explore the forming mechanism of hydrogen production, we analyzed the potential structural and morphological transformations during photocatalytic reaction process for pure TiO$_2$, Pt$_1$-TiO$_2$, and Pt-NP-TiO$_2$ samples through the Ex-situ HRTEM and XRD characterizations. As shown in Fig. 3a, the margin configurations of TiO$_2$ catalysts have hardly changed after photo-reduction for 2 h in contrast to the pristine state. The lattice fringes in both edge and inner are well-defined without noticeable distortion and defects (Fig. S12). This state can be still maintained with the duration of light illumination to 10 h (Fig. S13). Similar results could also be gleaned from Pt-NP-TiO$_2$ samples (Fig. 3c and S14), in which the clear interface between Pt nanoparticles and TiO$_2$ matrix reveals the close linkage status after photocatalytic reaction for 2 h. When further prolonging the catalytic time to 10 h, the boundary and lattices still remain clear and well-organized (Fig. S15). However, the Pt$_1$-TiO$_2$ catalyst exhibits quite different surface structures from those of TiO$_2$ and Pt-NP-TiO$_2$. As shown in Fig. 3b, a disordered surface layer with about 2 nm thickness generated after reacting 2 h, resulting into a notable rugged edge
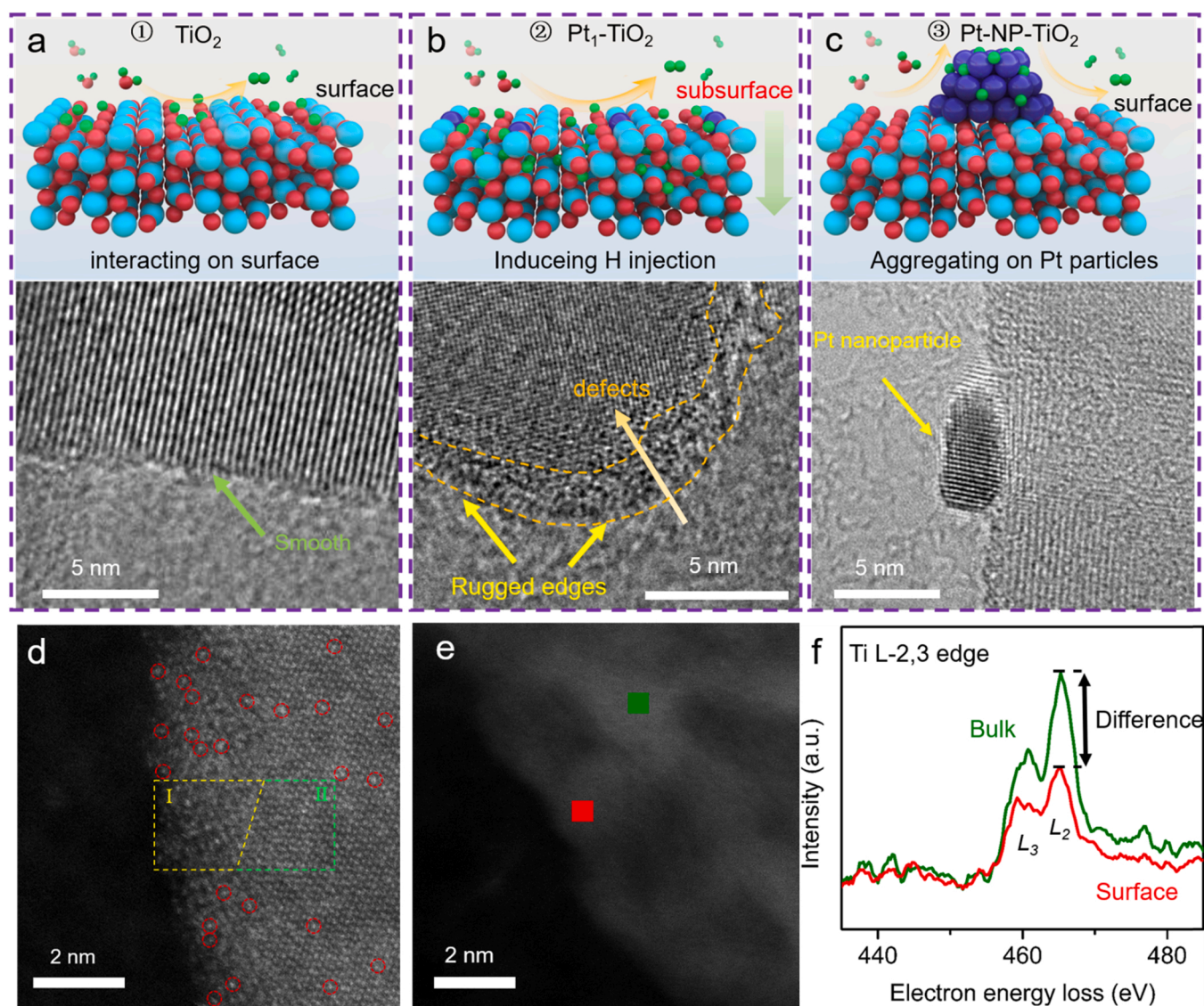
Fig. 3. The schematic illustrations and HRTEM images of (a) TiO$_2$, (b) Pt$_1$-TiO$_2$, (c) Pt-NP-TiO$_2$ after photocatalytic hydrogen evolution for 2 h. The hydrogen, platinum, titanium and oxygen atoms are colored in green, purple, blue and red, respectively. (d) The HAADF-STEM image of Pt$_1$-TiO$_2$ after photocatalytic reactions (for 2 h). The amorphous shell is marked by yellow frame (I) and the crystalline inner region is marked by green frame (II). (e) The HAADF image of Pt$_1$-TiO$_2$ after photocatalytic reactions (for 2 h). (f) The EELS results were extracted from the surface (red dot in (e)) and the inner (green dot in (e)), respectively.

configuration (Fig. S16). However, the bulk region still retains original crystal structure without obvious change, and thus leading an ordered core/disordered shell morphology. Impressively, this unique structure still exists and maintains unchanged when the illumination time extended to 10 h (Fig. S17). In addition, the distorted edge structure will spontaneously introduce amounts of crystal defects along layer surface, which indicates that vacancies could transfer from Pt_1-TiO_2 surface towards the bulk center during photo-reduction process. To further intuitively demonstrate the surface configuration and valence state changes, the HAADF-STEM and electron energy loss spectroscopy (EELS) measurements were performed. As seen in Fig. 3d, the bright dots marked by red circles can be identified as Pt single atoms over the whole Pt_1-TiO_2 NSs, suggesting the Pt species still keeps single dispersive status after photocatalytic reaction. Obviously, the TiO_2 edge with about 2 nm thickness (yellow frame) converts into disordered configuration compared to the intact bulk centers (green frame), according well with the HRTEM results. More compared zones were displayed in Fig. S18. Moreover, the Ti qualitative interpretation of electronic states for both surface (red dot in Fig. 3e) and bulk (green dot in Fig. 3e) were recorded by the EELS analysis. As shown in Fig. 3f, the Ti L_3 peak recorded from the surface shifts to lower energies relative to the bulk position, indicating the presence of lower Ti electronic states on the surface, such as, Ti^{3+} [29]. The noticeable decrease of Ti L_2 and L_3 peak intensity mainly

is ascribed to the generation of defects [30]. Therefore, according to the above morphological transformations and valence state changes results, we propose that the surface single Pt atoms trend to induce the hydrogen injection into the TiO_2 subsurface to generate self-hydrogenated shell and thus entice the formation of defects. For pure TiO_2 catalysts, the formation and desorption of hydrogen during photocatalytic process are inclined to interact on the surface. When loading Pt nanoparticles onto the surface, the photo-excited electrons from TiO_2 conduction band can be transferred to Pt nanoparticles, resulting into the adsorption and activation of hydrogen predominantly focus on Pt nanoparticles, in accordance with previous reports [21]. Since the Pt nanoparticles possess stronger adsorption ability of hydrogen, the hydrogen injection process may not be triggered when the Pt nanoparticles/clusters and Pt single atoms are coexisting on the surface. The control experiment in Fig. S19 exhibits both Pt clusters (purple frame) and Pt single atoms (red circle) loading on the 1.25% wt% Pt-TiO_2 supports after photocatalytic reaction 2 h. Consistent with our inferences, no notably disordered edge shell structures were found, indicating the predominant hydrogen evolution concerns on Pt clusters.

3.4. DFT calculations

To further illustrate the critical role of hydrogenated shell in
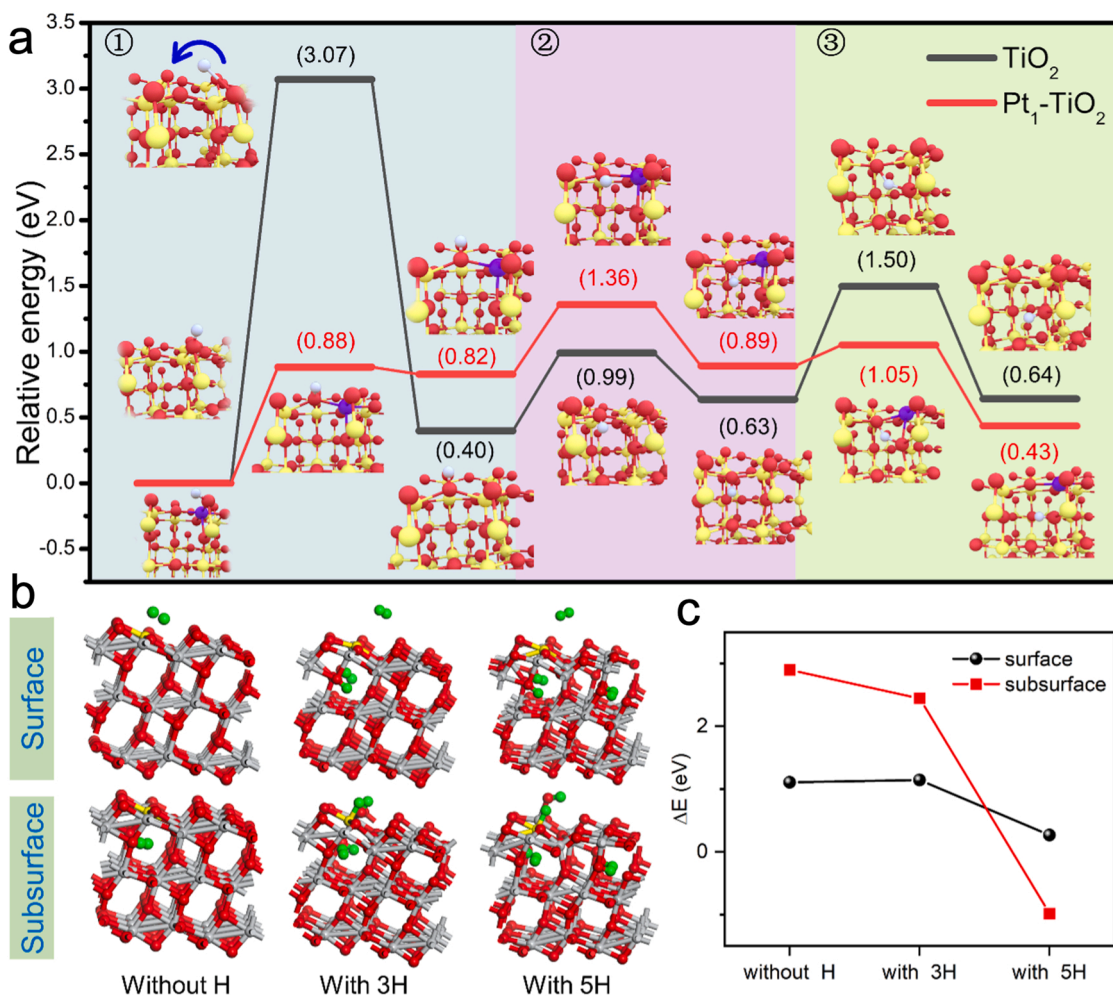
Fig. 4. (a) The comparison of the hydrogen injection for TiO_2 and Pt_1-TiO_2 catalysts. ①the diffusion and migration of H atoms; ②the transfer of H atoms into the subsurface; ③the stability of H atoms for the formation of hydrogenated shell. The hydrogen, platinum, titanium and oxygen atoms are colored in white, purple, yellow and red, respectively. (b) The H_2 formation process on various of hydrogen-adsorbed Pt_1-TiO_2 configurations. "Without H", "With 3 H" and "With 5 H" mean that the subsurface of Pt_1-TiO_2 contains 1, 3 and 5 hydrogen atoms adsorbed on the oxygen atoms. The hydrogen, platinum, titanium and oxygen atoms are colored in green, yellow, gray and red, respectively. (c) Desorption energies for the process of H_2 formation on the Pt_1-TiO_2 (101) surface or subsurface with different hydrogen-adsorbed concentrations.

photocatalytic hydrogen evolution process, the first-principle calculations were conducted. As seen in Fig. 4a, there are three possible steps happened in catalysts surface including ①the diffusion and migration of H atoms; ②the permeation of H atoms into the subsurface; ③the stability of H atoms for the formation of hydrogenated shell. In step 1, the initial hydrogen atom is adsorbed on outmost bridging oxygen and then migrates to adjacent three-coordinated oxygen (O_{3c}) away from the surface. Especially, the energy barrier in Pt_1-TiO_2 surface is far below than that in TiO_2 surface, suggesting the diffusion of hydrogen to the subsurface is much easier in the presence of Pt single atoms. Then, the H atom rotates along the O_{3c} into the inner of bulk crystal (step 2) and keep stable in subsurface (step 3). Compared with H atom stabilized in TiO_2 subsurface, the overall barrier is obviously reduced from 1.50 to 1.05 eV when the H atom locates in the Pt_1-TiO_2 subsurface, indicating the hydrogen is much easier to stabilize in the Pt_1-TiO_2 subsurface. Therefore, the DFT calculations support that single atom Pt in TiO_2 surface can effectively facilitate the permeation of hydrogen to the subsurface and ultimately induce the formation of hydrogenated shell, which agrees well with our experimental observation. Moreover, the desorption energies of hydrogen on the Pt_1-TiO_2 (101) surface and subsurface with different hydrogen-adsorbed concentrations are showed in Fig. 4b. Obviously, the desorption energy of hydrogen on the subsurface significantly decreases when increasing the hydrogen concentrations to five-covered hydrogen atoms, which is pronouncedly lower than hydrogen forming on the surface (Fig. 4c). The same results can be also found in the oxygen-defect Pt_1-TiO_2 configurations in Fig. S20. This further indicates the hydrogenated Pt_1-TiO_2 shell is beneficial to the hydrogen desorption for the H_2 formation process (Fig. S21). In addition, the ab initio molecular dynamics (AIMD) simulation was further carried out at 300 K (Movie 1 and Fig. S22). After 8 ps, two adjacent hydrogen atoms combine with one lattice oxygen atom to form water molecular inside the hydrogenated TiO_2 slab, resulting into the formation of oxygen defects and low-state Ti species, which agrees well with our experimental observation that hydrogenated shell is still existing after photocatalytic H_2 evolution reaction.

Supplementary material related to this article can be found online at doi:10.1016/j.apcatb.2022.122303.

4. Conclusion

In summary, we have investigated different surface actions based on metal Pt on TiO_2 surface during photocatalytic hydrogen evolution process. Experimental results exhibited that single Pt atoms could induce the formation of self-hydrogenated shell during photocatalytic reactions, while no obvious surface changes in both bare TiO_2 and Pt nanoparticles loading TiO_2 NSs catalysts. The synthetic Pt_1-TiO_2 catalysts show excellent photocatalytic activity of 42.9 mmol $g^{-1} h^{-1}$, which is 86 times higher activity than pure TiO_2 and surpasses that of most known photocatalysts. Density functional theory calculations further verify that single Pt atoms on TiO_2 surface can effectively transfer the hydrogen to subsurface and induce the formation of hydrogenated shell, which significantly reduces the desorption energies of H_2 formation. This discovery provides important insight for hydrogen evolution reactions on TiO_2 and Pt/TiO_2 surface and is also expected to open up a new way to design highly effective photocatalysts.

CRediT authorship contribution statement

Zhenggang Xue: Methodology, Data curation, Formal analysis, Writing – original draft. **Muyu Yan**: Writing – review & editing. **Yida Zhang**: XANES and EXAFS spectrometry analyses. **Jiaqiang Xu**: Writing – review & editing. **Xiaoping Gao**: Performing the DFT calculations. **Yuen Wu**: Conceiving and designing the research.

Declaration of Competing Interest

The authors declare that they have no known competing financial interests or personal relationships that could have appeared to influence the work reported in this paper.

Data availability

Data will be made available on request.

Appendix A. Supporting information

Supplementary data associated with this article can be found in the online version at doi:10.1016/j.apcatb.2022.122303.

References

[1] C.M. Wolff, P.D. Frischmann, M. Schulze, B.J. Bohn, R. Wein, P. Livadas, M. T. Carlson, F. Jäckel, J. Feldmann, F. Würthner, J.K. Stolarczyk, All-in-one visible-light-driven water splitting by combining nanoparticulate and molecular co-catalysts on CdS nanorods, Nat. Energy 3 (2018) 862–869.

[2] S.J.A. Moniz, S.A. Shevlin, D.J. Martin, Z.-X. Guo, J. Tang, Visible-light driven heterojunction photocatalysts for water splitting-a critical review, Energy Environ. Sci. 8 (2015) 731–759.

[3] M. Guo, M. Zhang, R. Liu, X. Zhang, G. Li, State-of-the-Art advancements in photocatalytic hydrogenation: reaction mechanism and recent progress in Metal-organic framework (MOF)-based catalysts, Adv. Sci. 9 (2022), e2103361.

[4] D. Gao, J. Xu, L. Wang, B. Zhu, H. Yu, J. Yu, Optimizing atomic hydrogen desorption of sulfur-rich NiS_{1+x} cocatalyst for boosting photocatalytic H_2 evolution, Adv. Mater. 34 (2022), e2108475.

[5] Y. Yang, L.C. Yin, Y. Gong, P. Niu, J.Q. Wang, L. Gu, X. Chen, G. Liu, L. Wang, H. M. Cheng, An unusual strong visible-light absorption band in red anatase TiO_2 photocatalyst induced by atomic hydrogen-occupied oxygen vacancies, Adv. Mater. 30 (2018) 1704479.

[6] Q. Guo, C. Zhou, Z. Ma, X. Yang, Fundamentals of TiO_2 photocatalysis: concepts, mechanisms, and challenges, Adv. Mater. 31 (2019), e1901997.

[7] H. Zhao, Z. Jiang, K. Xiao, H. Sun, H.S. Chan, T.H. Tsang, S. Yang, P.K. Wong, Photo-assisted separation of noble-metal-free oxidation and reduction cocatalysts for graphitic carbon nitride nanosheets with efficient photocatalytic hydrogen evolution, Appl. Catal. B Environ. 280 (2021) 119456.

[8] L. Zhang, B.K. Miller, P.A. Crozier, Atomic level in situ observation of surface amorphization in anatase nanocrystals during light irradiation in water vapor, Nano Lett. 13 (2013) 679–684.

[9] H. Hussain, G. Tocci, T. Woolcot, X. Torrelles, C.L. Pang, D.S. Humphrey, C.M. Yim, D.C. Grinter, G. Cabailh, O. Bikondoa, R. Lindsay, J. Zegenhagen, A. Michaelides, G. Thornton, Structure of a model TiO_2 photocatalytic interface, Nat. Mater. 16 (2017) 461–466.

[10] Y. He, A. Tilocca, O. Dulub, A. Selloni, U. Diebold, Local ordering and electronic signatures of submonolayer water on anatase $TiO_2(101)$, Nat. Mater. 8 (2009) 585–589.

[11] O. Bikondoa, C.L. Pang, R. Ithnin, C.A. Muryn, H. Onishi, G. Thornton, Direct visualization of defect-mediated dissociation of water on $TiO_2(110)$, Nat. Mater. 5 (2006) 189–192.

[12] D. Gao, J. Xu, F. Chen, P. Wang, H. Yu, Unsaturated selenium-enriched $MoSe_{2+x}$ amorphous nanoclusters: one-step photoinduced co-reduction route and its boosted

photocatalytic H$_2$-evolution activity for TiO$_2$, Appl. Catal. B Environ. 305 (2022), 121053.

[13] W. Zhong, D. Gao, P. Wang, X. Wang, H. Yu, Accelerating hydroxyl desorption by swapping catalytic sites in RuMoS$_{2+x}$ cocatalysts for efficient alkaline photocatalytic H$_2$ production, Appl. Catal. B Environ. 319 (2022), 121910.

[14] D. Gao, B. Zhao, L. Wang, E. Aslan, I. Hatay Patir, J. Yu, H. Yu, Electron-enriched regulation of sulfur-active site for accelerating atomic hydrogen desorption of S-rich MoWS$_{2+x}$ cocatalyst toward efficient photocatalytic H$_2$ evolution of TiO$_2$, Chem. Eng. J. 449 (2022), 137803.

[15] J. Feng, C. An, L. Dai, J. Liu, G. Wei, S. Bai, J. Zhang, Y. Xiong, Long-term production of H$_2$ over Pt/CdS nanoplates under sunlight illumination, Chem. Eng. J. 283 (2016) 351–357.

[16] M. Ni, M.K.H. Leung, D.Y.C. Leung, K. Sumathy, A review and recent developments in photocatalytic water-splitting using TiO$_2$ for hydrogen production, Renew. Sustain. Energy Rev. 11 (2007) 401–425.

[17] S. Hejazi, S. Mohajernia, B. Osuagwu, G. Zoppellaro, P. Andryskova, O. Tomanec, S. Kment, R. Zboril, P. Schmuki, On the controlled loading of single Platinum atoms as a co-catalyst on TiO$_2$ Anatase for optimized photocatalytic H$_2$ generation, Adv. Mater. 32 (2020), e1908505.

[18] W. Li, X.-s Chu, F. Wang, Y.-y Dang, X.-y Liu, T.-h Ma, J.-y Li, C.-y Wang, Pd single-atom decorated CdS nanocatalyst for highly efficient overall water splitting under simulated solar light, Appl. Catal. B Environ. 304 (2022), 121000.

[19] S. Qiu, Y. Shen, G. Wei, S. Yao, W. Xi, M. Shu, R. Si, M. Zhang, J. Zhu, C. An, Carbon dots decorated ultrathin CdS nanosheets enabling in-situ anchored Pt single atoms: a highly efficient solar-driven photocatalyst for hydrogen evolution, Appl. Catal. B Environ. 259 (2019), 118036.

[20] J. Shen, R. Fan, Y. Wang, J. Zhou, C. Chen, Z. Wei, S. Ju, T. Qian, Y. Peng, M. Shen, Oxygen-vacancy-rich nickel hydroxide nanosheet: a multifunctional layer between Ir and Si toward enhanced solar hydrogen production in alkaline media, Energy Environ. Sci. 15 (2022) 3051–3061.

[21] Y. Lu, W.J. Yin, K.L. Peng, K. Wang, Q. Hu, A. Selloni, F.R. Chen, L.M. Liu, M.L. Sui, Self-hydrogenated shell promoting photocatalytic H$_2$ evolution on anatase TiO$_2$, Nat. Commun. 9 (2018) 2752.

[22] L. Wang, W. Chen, D. Zhang, Y. Du, R. Amal, S. Qiao, J. Wu, Z. Yin, Surface strategies for catalytic CO$_2$ reduction: from two-dimensional materials to nanoclusters to single atoms, Chem. Soc. Rev. 48 (2019) 5310–5349.

[23] X. Li, J. Yu, M. Jaroniec, X. Chen, Cocatalysts for selective photoreduction of CO$_2$ into solar fuels, Chem. Rev. 119 (2019) 3962–4179.

[24] J. Li, H. Huang, W. Xue, K. Sun, X. Song, C. Wu, L. Nie, Y. Li, C. Liu, Y. Pan, H.-L. Jiang, D. Mei, C. Zhong, Self-adaptive dual-metal-site pairs in metal-organic frameworks for selective CO$_2$ photoreduction to CH$_4$, Nat. Catal. 4 (2021) 719–729.

[25] G. Wang, R. Huang, J. Zhang, J. Mao, D. Wang, Y. Li, Synergistic modulation of the separation of photo-generated carriers via engineering of dual atomic sites for promoting photocatalytic performance, Adv. Mater. 33 (2021), e2105904.

[26] Y. Yang, P. Gao, X. Ren, L. Sha, P. Yang, J. Zhang, Y. Chen, L. Yang, Massive Ti^{3+} self-doped by the injected electrons from external Pt and the efficient photocatalytic hydrogen production under visible-light, Appl. Catal. B Environ. 218 (2017) 751–757.

[27] D. Jiang, D. Zhou, Q. Zhang, Q. Song, C. Zhou, X. Shi, D. Li, Synergistic integration of AuCu co-catalyst with oxygen vacancies on TiO$_2$ for efficient photocatalytic conversion of CO$_2$ to CH$_4$, ACS Appl. Mater. Interfaces 13 (2021) 46772–46782.

[28] C.Y. Li, J.B. Le, Y.H. Wang, S. Chen, Z.L. Yang, J.F. Li, J. Cheng, Z.Q. Tian, In situ probing electrified interfacial water structures at atomically flat surfaces, Nat. Mater. 18 (2019) 697–701.

[29] L. Li, J. Yan, T. Wang, Z.J. Zhao, J. Zhang, J. Gong, N. Guan, Sub-10 nm rutile titanium dioxide nanoparticles for efficient visible-light-driven photocatalytic hydrogen production, Nat. Commun. 6 (2015) 5881.

[30] A. Naldoni, M. Allieta, S. Santangelo, M. Marelli, F. Fabbri, S. Cappelli, C.L. Bianchi, R. Psaro, V. Dal Santo, Effect of nature and location of defects on bandgap narrowing in black TiO$_2$ nanoparticles, J. Am. Chem. Soc. 134 (2012) 7600–7603.